JOURNAL OF SPACECRAFT AND ROCKETS
Vol. 46, No. 4, July–August 2009

Transfer Trajectories Design for a Variable Lightness Solarcraft

Shengping Gong,* Junfeng Li,† and Hexi Baoyin‡
Tsinghua University, 100084 Beijing, People's Republic of China

DOI: 10.2514/1.34886

A new configuration of sailcraft that can adjust its lightness number is proposed in this paper. The new-concept sailcraft can evolve along different displaced solar orbits passively. Transfer trajectories between different displaced orbits are investigated, and two different strategies are employed to complete the transfers. When the initial and final orbits are close to each other, a linear model is used to generate an analytical control law first and it is corrected differentially to control the nonlinear model. The transfer accuracy at the target point can be specified in the differential corrections process. Numerical examples are employed to validate the control method over the transfer arc. The results show that the convergence becomes worse as the distance between the two orbits increases until the iteration process does not lead to the desired result when the distance between two orbits is outside the linear range. For these cases, a direct optimization method is employed for transfer trajectory design. The transfer trajectory is divided into segments, and the control law is assumed constant over each segment. Then, the design problem is transformed into a parameter optimization problem. A genetic algorithm and a conjugate gradient method are combined to achieve the desired results. The method proposed in this investigation proved efficient over the range of cases considered.

Nomenclature

C_m = center of mass of the sailcraft
C_p = center of solar radiation pressure of the sailcraft
$\boldsymbol{F}_1$ = resultant solar radiation pressure force exerted on S_1 and S_2
$\boldsymbol{F}_2$ = resultant solar radiation pressure force exerted on S_3 and S_4
h_i = distance from the apex to the center of mass of S_i ($i = 1, 2, 3, 4$)
L = length of the boom used to support the payload
M_t = total mass of the sailcraft
m_b = mass of bus
m_p = mass of payload
$\boldsymbol{n}$ = force vector along the sail normal axis
$\boldsymbol{n}_i$ = unit normal vector of S_i
$\boldsymbol{n}_s$ = unit normal vector of solar light
O = the intersection point of S_i ($i = 1, 2, 3, 4$)
O_i = the mass center of S_i ($i = 1, 2, 3, 4$)
P_1 = center of pressure of S_1 and S_2
P_2 = center of pressure of S_3 and S_4
r = distance from the sail to the sun
$\boldsymbol{r}_{AB}$ = vector from point A to point B
$\boldsymbol{r}_{C_mC_p}$ = vector from point C_m to C_p
S_i = area of a specific sail ($i = 1, 2, 3, 4$) in the cone configuration consisting of four sails
z_0 = displacement of the displaced orbit
α_i = angle between $\boldsymbol{n}_s$ and $\boldsymbol{n}_i$
β_c = lightness number of the whole sailcraft
β_s = lightness number of the sail
γ_1 = angle between S_1 and S_2
γ_2 = apex angle of S_1 and S_2
θ_1 = angle between S_3 and S_4
θ_2 = apex angle of S_3 and S_4
$\boldsymbol{\lambda}$ = the costate of the optimal control
μ = solar gravitational constant
σ = density of the sail, $\mathrm{kg/m^2}$
ρ_0 = radius of the displaced orbit
ψ = the deviation from the equilibrium position in the direction perpendicular to the plane formed by $\boldsymbol{r}_0$ and z
$\boldsymbol{\omega}_0$ = angular velocity vector of the sailcraft

Introduction

THE concept of solar sails for space flight was proposed in 1921. Since then, solar sail technology has greatly advanced. Many applications for solar sails have been proposed in recent years. For instance, the GeoSail mission seeks to explore the geomagnetic tail [1]. Similarly, the Geostorm Warning mission seeks to place a spacecraft at a sail-controlled artificial Lagrange point that is used to provide early warning during solar plasma storms [2,3]. Other missions envision the solar sail along a displaced solar orbit to observe the polar area of the Earth. A displaced solar orbit is a periodic non-Keplerian circular orbit first proposed by Forward in 1981 [4]. In a two-body problem, a sailcraft under the influences of solar gravity and solar radiation pressure can be displaced above the ecliptic plane. The orbit period, orbit radius, and out-of-plane displacement distance may be chosen independently with a suitable choice of solar sail pitch angle and lightness number [5]. McInnes [6,7] identified large families of displaced orbits by considering the dynamics of a sailcraft in a rotating frame, for which the x and y axes are in the ecliptic plane and which rotates along z axis synchronously with the displaced orbit. In these studies, the dynamics, stability, and control of different families of displaced orbits were investigated.

At present, several sailcraft configurations are proposed for various missions, including a heliogyro, a circular sail, and a square sail, as shown in Fig. 1a. The heliogyro and circular sail are passively spin stabilized. The square sail requires active attitude control systems. The heliogyro configuration, adopted by Cosmos 1, did not achieve its intended goal due to an unrelated hardware failure [8]. The square sail concept, adopted by NASA and ESA, was also considered in previous studies [9,10]. Several ground validation experiments have been conducted on the deployment, modal testing [11], and attitude control system [12–14] among others. However, the size of the sail tested is limited by the size of the vacuum chamber available. Thus, large solar sails cannot be tested on Earth; subsequently, it is not possible to validate their performance and characteristics before launch. Simulation tools are available to predict the characteristics of large sails [15]. These can be validated by experiments on small sails on Earth. However, the similarity between small and large sails proves superficial and the dynamical characteristics of the small sails cannot be extended to large sails.

Received 4 December 2007; revision received 9 February 2009; accepted for publication 17 April 2009.

*Ph.D. Candidate, School of Aerospace; gsp04@mails.tsinghua.edu.cn.
†Professor, School of Aerospace; lijunf@tsinghua.edu.cn.
‡Associate Professor, School of Aerospace; baoyin@tsinghua.edu.cn. Member AIAA.

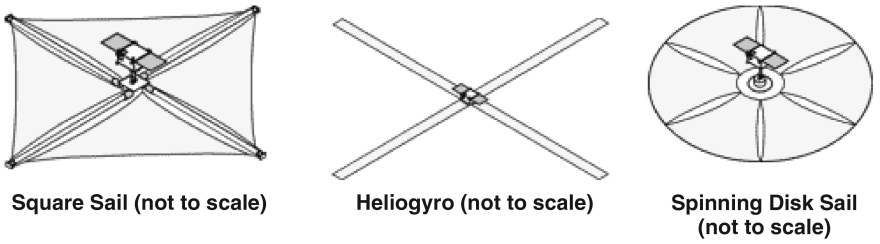

a) Three typical configurations

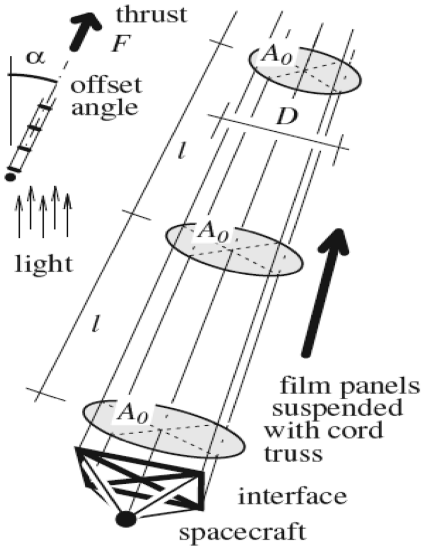

b) Space tow

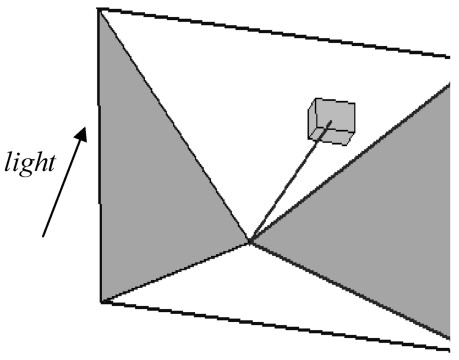

c) Cone configuration

Fig. 1 Different sail configurations.

Instead, Gyula [16] and Gyula and Edward [17] proposed a scalable concept, space tow. The space tow is proposed to avoid the scalability issues of a solar sail. The reasons for the delays that have been plaguing photon sail development are not only financial in nature. Solar sail engineering has been facing an array of technological bottlenecks, most of which are dimensional in nature. The idea of breaking up the reflecting surface into smaller pieces naturally followed, leading to the definition of the space tow, as shown in Fig. 1b, wherein the multitude of small pieces (panels) constitute the floors in a filament truss column. The pressure on each panel combines with the rest along the truss, together exerting the thrust on the payload attached to the rear end of the assembly. However, the concept introduces some other difficulties, such as control issues. Other studies [18] consider a three-dimensional positive cone as a sail concept, as shown in Fig. 1c. The coupled attitude–orbit dynamics is considered simultaneously, and the results indicate this sailcraft can be passively stabilized along the displaced solar orbit by designing parameters of the cone configuration. With a proper design, restoring forces and torques are generated to stabilize the attitude and orbit in the presence of deviations relative to the equilibrium position. In this case, the sail angles change periodically in the inertial frame while remaining fixed in the rotating frame.

All the configurations usually exhibit a common characteristic, that is, the lightness number of the sailcraft is fixed. However, the ability to vary the lightness number of a sailcraft is critical for some missions. For example, the ability to vary the sail lightness number is necessary for a mission requiring the sailcraft to work at different displaced orbits, because different orbits have different requirements on the lightness number [19].

This investigation focuses on two topics: first, a new variable lightness number configuration is proposed; and second, algorithms to design the transfer trajectory between different displaced solar orbits are investigated based on this configuration. In the previous literature, most of the proposed sailcraft assume fixed configurations and a fixed lightness number. To improve the adaptability, a positive cone sailcraft with four adjustable quadrant sails is proposed in this paper. When the sailcraft is in a "loose" state, its configuration is similar to that of Cosmos 1 [20], consisting of eight separate sails. When the sailcraft is in a "tight" state, its four quadrant sails form a positive cone. The sailcraft can be passively stable on different displaced orbits in different "locked" states. The parameters of the stable locked state are obtained by designing the relative positions of different parts using the design method employed by Gong et al. [18]. A locked state implies that the relative positions of each part of the sailcraft remain fixed. For a given displaced orbit, a corresponding locked state can be designed to guarantee sailcraft stability without active control. For a mission that requires the sailcraft to be passively stable along different orbits, this kind of configuration is useful. The sailcraft can work on one orbit for a period of time and then work on another orbit. The transfer arc between two orbits can be achieved by adjusting its attitude angles. Control algorithms are necessary to complete the transfer arc. In this study, two methodologies are discussed with regard to the transfer between different displaced orbits. In the first method, the linearized dynamics of the sailcraft is used. As a result, this scheme is only applicable in the immediate vicinity of the initial orbit. A control law is initially derived from the linearized model, and a differential corrections process is employed to transition the results into the true nonlinear model. In the second method, a near optimal transfer, and associated control history, is determined through the use of genetic algorithms. This is most suitable when the distance between the orbits is outside the linear range. The direct method is suitable for preliminary analyses of solar sail missions because the attitude of the sail is fixed over each trajectory segment, similar to a bang–bang control law. Therefore, only a few changes in attitude are required during the transfer.

Displaced Solar Orbits

When the sailcraft is far from the Earth, the gravitational forces of the Earth exerted on the sailcraft are negligible because they are very

small in contrast to the solar gravity and solar radiation pressure. For orbits near the Earth, the gravity of the Earth has a greater influence, a case that is not considered here. In this paper, a two-body problem model is adopted. The frame O_iXYZ in Fig. 2 is an inertial frame. A rotating frame is also defined such that the origin is located at the sun, the x axis points from the sun to the projection point of the sailcraft on the ecliptic, the z axis is normal to the ecliptic, and the y axis completes a right-hand frame. This frame rotates around the z axis with an angular velocity of ω_0. In the rotating frame, the equation of motion of an ideal planar sail may be formulated as

$$\ddot{\boldsymbol{r}} + 2\boldsymbol{\omega}_0 \times \dot{\boldsymbol{r}} + \boldsymbol{\omega}_0 \times (\boldsymbol{\omega}_0 \times \boldsymbol{r}) = -\frac{\mu}{r^3}\boldsymbol{r} + \beta\frac{\mu}{r^4}(\boldsymbol{r}\cdot\boldsymbol{n}_0)^2\boldsymbol{n}_0 \quad (1)$$

The location of the equilibrium point, in the rotating frame, associated with the desired displaced orbit, in the inertial frame, is characterized by radius ρ_0, displacement z_0 relative to the ecliptic plane, and orbital angular velocity ω_0. The sail pitch angle α and sail lightness number β are determined by the displaced solar orbit and are given by [7]

$$\tan\alpha = \frac{\frac{z_0}{\rho_0}\left(\frac{\omega_0}{\tilde{\omega}}\right)^2}{\left(\frac{z_0}{\rho_0}\right)^2 + 1 - \left(\frac{\omega_0}{\tilde{\omega}}\right)^2} \quad (2)$$

$$\beta = \left[1 + \left(\frac{z_0}{\rho_0}\right)^2\right]^{\frac{1}{2}} \frac{\left\{\left(\frac{z_0}{\rho_0}\right)^2 + \left[1 - \left(\frac{\omega_0}{\tilde{\omega}}\right)^2\right]^2\right\}^{\frac{3}{2}}}{\left[\left(\frac{z_0}{\rho_0}\right)^2 + 1 - \left(\frac{\omega_0}{\tilde{\omega}}\right)^2\right]^2} \quad (3)$$

where $\tilde{\omega}^2 = \mu/r_0^3$, $r_0^2 = \rho_0^2 + z_0^2$.

As mentioned earlier, a displaced solar orbit is a circular sun-centered orbit displaced above the ecliptic plane by directing a component of the solar radiation pressure force in a direction normal to the ecliptic plane. For an ideal planar sail, the sail orientation is defined by its normal vector $\boldsymbol{n}_0$, fixed in a rotating frame, as shown in Fig. 2. The performance of the sailcraft is characterized by the sail lightness number, related to the density of the sail by [7]

$$\beta_c = (1.53/\sigma) \times 10^{-3} \quad (4)$$

Equation (4) is valid for all sail design.

Sailcraft Configuration

A four-triangle-form sail configuration is adopted in this paper, as shown in Fig. 3. The sailcraft is composed of four sails shaped as isosceles triangles. It also includes a bus positioned at the common apex of the sails and a payload located at the end of a massless boom. The sail parameters are S_i $(i = 1, 2, 3, 4)$, $\gamma_1, \theta_1, \gamma_2, \theta_2, \sigma, m_p$, and m_b.

In this paper, the sail geometry is selected such that $S_i = S$ $(i = 1, 2, 3, 4)$ and $\gamma_2 = \theta_2$. As shown in Fig. 3, two different states with different angles between the opposed sails will be discussed. For a tight state, four sails form a positive cone with the angle between the opposed sails defined as $\gamma_{\min}$, assumed to be the smallest angle for all the states of the sailcraft. The assumption is based on the premise that one sail may be in the shaded region of another one for a smaller value

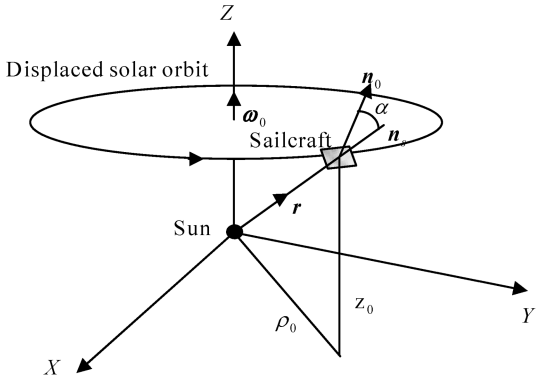

Fig. 2 Displaced solar orbit.

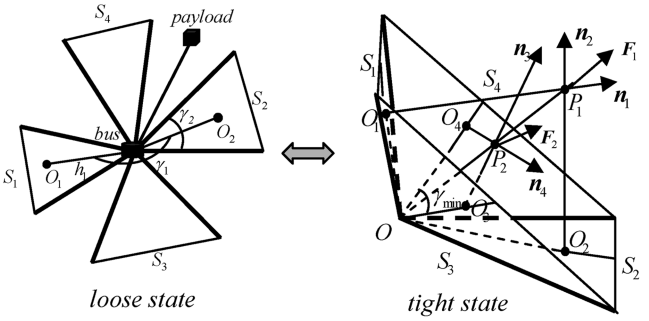

Fig. 3 Different states of the sailcraft.

of γ_1 or θ_1. For a loose state, the sails are like the vanes of an electric fan, and the angles between the opposed sails, which can be set differently from the other opposing pair, are larger than the critical angle, namely, $\gamma_1 \geq \gamma_{\min}$ and $\theta_1 \geq \gamma_{\min}$, where $\gamma_{\min}$ can be calculated for a given γ_2, $\gamma_{\min} = 2\sin^{-1}[(\sqrt{2}/2)/\cos(\gamma_2/2)]$.

The center of pressure of the resultant forces of the two opposing quadrant sails is the intersection point of their normal vectors, as shown in Fig. 3. Therefore, the resultant total solar pressure acceleration is determined as

$$\boldsymbol{F}_s = \boldsymbol{F}_1 + \boldsymbol{F}_2 \quad (5)$$

where

$$\boldsymbol{F}_1 = \sigma S\beta\mu\left[\frac{(\boldsymbol{n}_1\cdot\boldsymbol{n}_s)^2}{r^2}\boldsymbol{n}_1 + \frac{(\boldsymbol{n}_2\cdot\boldsymbol{n}_s)^2}{r^2}\boldsymbol{n}_2\right] \quad (6)$$

$$\boldsymbol{F}_2 = \sigma S\beta\mu\left[\frac{(\boldsymbol{n}_3\cdot\boldsymbol{n}_s)^2}{r^2}\boldsymbol{n}_3 + \frac{(\boldsymbol{n}_4\cdot\boldsymbol{n}_s)^2}{r^2}\boldsymbol{n}_4\right] \quad (7)$$

The resultant torque relative to the center of mass can be given by

$$\boldsymbol{M}_{c_m} = \boldsymbol{r}_{C_mC_p} \times \boldsymbol{F}_s \quad (8)$$

Different displaced orbits have different requirements for the lightness number and sail angle. For a sailcraft with fixed sails, the lightness number is fixed. Therefore, the sailcraft can only evolve on displaced orbits for which the lightness number is equal to the fixed value. The sailcraft configuration proposed in this study can possess different lightness numbers in different locked states.

The acceleration ability of a sailcraft is described by its lightness number, which is related to the lightness number of each sail and the total mass of the sailcraft. The solar radiation pressure acceleration exerted on the sailcraft can be given by

$$\boldsymbol{a}_s = (\boldsymbol{F}_1 + \boldsymbol{F}_2)/M_t \quad (9)$$

where $M_t = 4\sigma s + m_p + m_b$ is the total mass of the sailcraft.

For the sailcraft configuration considered here, S, γ_2, m_b, and m_p are constant. When the sailcraft evolves along a displaced orbit, the required solar pressure acceleration is in the plane spanned by $\boldsymbol{\omega}_0$ and $\boldsymbol{r}_0$. Therefore, the sails S_3, S_4 can be symmetrically arranged. However, in the plane spanned by $\boldsymbol{\omega}_0$ and $\boldsymbol{r}_0$, the direction of the required solar pressure acceleration $\boldsymbol{n}_0$ deviates from the direction of solar light $\boldsymbol{n}_s$. Therefore, the opposed sails S_1 and S_2 need to be asymmetrically placed. Subsequently, the following relation applies: $\alpha_3 = \alpha_4 = (\pi - \theta_1)/2$, $\alpha_1 + \alpha_2 = \pi - \gamma_1$. The acceleration $\boldsymbol{a}_s$ is a function of three independent variables, given by α_1, γ_1, and θ_1. The parameters, γ_1 and θ_1, are determined by the angular positioning of the sails; the parameter α_1 is determined by the attitude of the sailcraft. The definition of the lightness number of the sailcraft is given below; first, two angles used to describe the configuration of the sailcraft, γ_1 and θ_1, are fixed. Then, the angle α_1 is adjusted to maximize the solar radiation pressure acceleration. The ratio of the maximum solar radiation pressure acceleration to the solar gravitational acceleration is defined as its lightness number. The

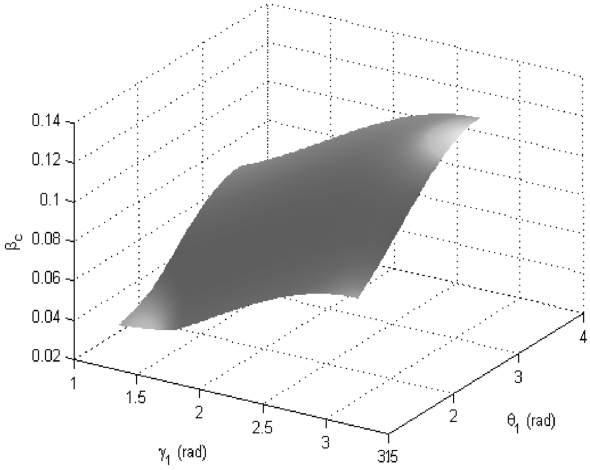

Fig. 4 Lightness number for different states.

lightness number of the sailcraft is independent of the angle α_1 and is determined by the angles between opposed sails, γ_1 and θ_1. If the parameters, and θ_1, are fixed, according to the definition of the lightness number, the lightness number of the sailcraft can be obtained as

$$\beta_c = \max_{\alpha_1} \frac{(\boldsymbol{F}_1 + \boldsymbol{F}_2)}{M_t(\mu/r^2)} \tag{10}$$

Notationally, $\max_{\alpha_1} f(\alpha_1)$ implies that $f(\alpha_1)$ is maximized with respect to α_1.

Figure 4 illustrates the relation between the lightness number, γ_1 and θ_1 based on the fixed parameters in Table 1, and the ranges of γ_1 and θ_1 in $(\gamma_{\min}, \pi)$. The minimum and maximum lightness numbers are determined as 0.03569 and 0.13113, respectively. The displaced orbit with an angular velocity equal to that of Earth is denoted as an Earth-synchronous displaced orbit. The Earth-synchronous displaced solar orbit that requires a lightness number in this range is determined from the shadowed region in Fig. 5.

For passive stability design, the attitude equilibrium position should be the attitude required to generate the orbit. To passively stabilize the sailcraft along a displaced solar orbit, two conditions should be satisfied. First, the design should ensure the force and moment balance when the sailcraft is located at the equilibrium position. Second, the sailcraft should generate a restoring force and torque when it deviates from the equilibrium position [18]. The sun, center of mass, and center of pressure are colinear when the sail is in equilibrium state. A restoring torque given by Eq. (8) is generated to pull the sail back to the equilibrium position if the sailcraft deviates from it. The design problem is converted into a parameter optimization problem and the sailcraft parameters are optimized [18] to satisfy the two conditions. The sailcraft can stabilize passively by designing the locked states as long as the orbit size parameters exist inside the shadowed region of Fig. 5. A sailcraft with the parameters given in Table 1 can evolve passively on different displaced orbits with different locked states. Five orbits are randomly selected from the shadowed region in Fig. 5, and the parameters of the corresponding passively stable locked state are given in Table 2.

If the sailcraft evolves along the initial orbit and the mission requires it to evolve along another orbit, the attitude of the sailcraft can be adjusted to accomplish the transfer. After the target orbit is achieved, the configuration of the sailcraft is locked to ensure that it is passively stable along the orbit again. Because the stability of the sailcraft along various orbits was previously addressed [18], this paper focuses on the transfer algorithm between displaced solar orbits.

Transfer Between Different Displaced Orbits

The transfer trajectory is achieved by actively adjusting the attitude of each sail. Four angles are employed to describe the configuration and attitude of the sailcraft in a loose state. The shape of the sails are determined by γ_1 and θ_1. The attitude of the sailcraft is determined by α_1 and ψ. These four angles are used here to navigate the sailcraft. In the rotating frame, the equation of motion of the sailcraft may be formulated as

$$\ddot{\boldsymbol{r}} + 2\boldsymbol{\omega}_0 \times \dot{\boldsymbol{r}} + \boldsymbol{\omega}_0 \times (\boldsymbol{\omega}_0 \times \boldsymbol{r}) = \boldsymbol{f}(\boldsymbol{r}) + \boldsymbol{g}(\boldsymbol{r}, \boldsymbol{n}_o^i) \tag{11}$$

where $\boldsymbol{r} = [x \quad y \quad z]^T$; $\boldsymbol{f}(\boldsymbol{r})$ is the gravitational force exerted by the sun, and $\boldsymbol{g}(\boldsymbol{r}, \boldsymbol{n}^i)$ represents solar pressure force.

$$\boldsymbol{f}(\boldsymbol{r}) = -(\mu/r^3)\boldsymbol{r} \tag{12}$$

$$\begin{aligned}\boldsymbol{g}(\boldsymbol{r}, \boldsymbol{n}^i) = (\sigma S \beta \mu / r^4)[&(\boldsymbol{n}_o^1 \cdot \boldsymbol{r})^2 \boldsymbol{n}_o^1 + (\boldsymbol{n}_o^2 \cdot \boldsymbol{r})^2 \boldsymbol{n}_o^2 + (\boldsymbol{n}_o^3 \cdot \boldsymbol{r})^2 \boldsymbol{n}_o^3 \\ &+ (\boldsymbol{n}_o^4 \cdot \boldsymbol{r})^2 \boldsymbol{n}_o^4]/[4\sigma S + m_b + m_s + m_p]\end{aligned} \tag{13}$$

In the rotating frame, the normal vectors of the four sails can be obtained as

$$\boldsymbol{n}_o^i = P\boldsymbol{n}_i \tag{14}$$

where

$$\boldsymbol{n}_1 = [\cos(\phi - \alpha_1)\cos\psi \quad \sin\psi \quad \sin(\phi - \alpha_1)\cos\psi]^T \tag{15}$$

$$\boldsymbol{n}_2 = [\cos(\pi + \phi - \alpha_1 - \gamma_1)\cos\psi \quad \sin\psi \quad \sin(\pi + \phi - \alpha_1 - \gamma_1)\cos\psi]^T \tag{16}$$

$$\boldsymbol{n}_3 = [\cos(\tfrac{\pi-\theta_1}{2} + \psi)\cos(\gamma - \alpha_1 - \tfrac{\gamma_1-\pi}{2}) \quad \sin(\tfrac{\pi-\theta_1}{2} + \psi) \quad \cos(\tfrac{\pi-\theta_1}{2} + \psi)\sin(\gamma - \alpha_1 - \tfrac{\gamma_1-\pi}{2})]^T \tag{17}$$

$$\boldsymbol{n}_4 = [\cos(\tfrac{\pi-\theta_1}{2} - \psi)\cos(\gamma - \alpha_1 - \tfrac{\gamma_1-\pi}{2}) \quad -\sin(\tfrac{\pi-\theta_1}{2} - \psi) \quad \cos(\tfrac{\pi-\theta_1}{2} - \psi)\sin(\gamma - \alpha_1 - \tfrac{\gamma_1-\pi}{2})]^T \tag{18}$$

Table 1 Sailcraft parameters

Parameter	Value
Sail density (σ)	0.01 kg/m^2
Bus mass (m_b)	20 kg
Payload (m_p)	20 kg
Sail area (S_0)	1500 m^2
Apex angle (γ_2)	$\pi/3$

$$P = \begin{bmatrix} \frac{x}{\sqrt{x^2+y^2}} & \frac{y}{\sqrt{x^2+y^2}} & 0 \\ \frac{y}{\sqrt{x^2+y^2}} & \frac{x}{\sqrt{x^2+y^2}} & 0 \\ 0 & 0 & 1 \end{bmatrix} \tag{19}$$

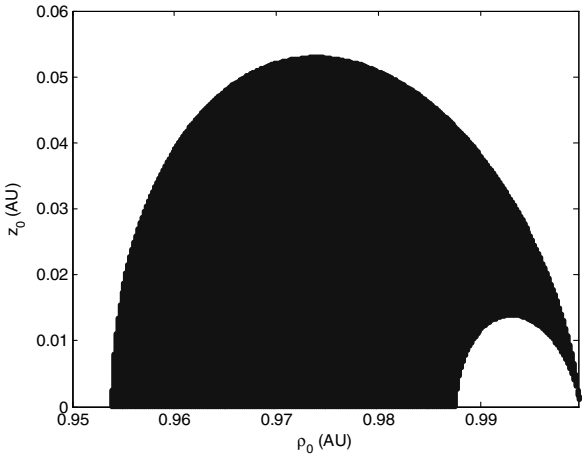

Fig. 5 Orbits on which the sailcraft can evolve.

$$\phi = \tan^{-1}(z_0/\rho_0) \tag{20}$$

A displaced orbit corresponds to an equilibrium point in the rotating frame. The transfer between different orbits is equivalent to a point-to-point transfer in the rotating frame. If the initial and target points are sufficiently close, the linearized model is sufficient to identify suitable transfer arcs. Otherwise, the nonlinear method is employed when identifying suitable transfer trajectories. The control variables are identified as $\boldsymbol{u} = [\,\gamma_1 \quad \theta_1 \quad \alpha_1 \quad \psi_1\,]^T$.

Linear Control Law

The equilibrium points of Eq. (11) correspond to a displaced orbit in the inertial frame. The dynamical equation of motion can be linearized around either the initial or target point. The linear equation is useful for transfer trajectory design between two close points. A traditional linear-quadratic regulator (LQR) algorithm is a good option for control design when the linearized dynamics provides a good approximation of the nonlinear behavior. Several authors use the LQR method for solar sail orbit control, including the control of displaced orbit [21,22] and periodic orbit in a restricted three-body model [23–25]. The control law is simple and controls the weak nonlinear model well. For the transfer trajectory in this paper, the implementation of the control law in the nonlinear model leads to transfer errors at the final time. To null the errors, a correction process is developed based on the linear dynamics. At last, a simple analytical control law for a nonlinear model can be obtained.

Now, in the rotating frame, the equations of motion are linearized in the vicinity of the equilibrium point. It is assumed that the solar sail can reach the target orbit through small variations of the control variables. Then, the translational equations of motion are linearized about the reference equilibrium state by introducing the following perturbed states: $\boldsymbol{r} \to \boldsymbol{r} + \delta\boldsymbol{r}, \boldsymbol{u} \to \boldsymbol{u} + \delta\boldsymbol{u}$. The linearized equations of motion are subsequently determined as

$$\delta\ddot{\boldsymbol{r}} + 2\boldsymbol{\omega}_0 \times \delta\dot{\boldsymbol{r}} + \boldsymbol{\omega}_0 \times (\boldsymbol{\omega}_0 \times \delta\boldsymbol{r}) = \frac{\partial \boldsymbol{f}(\boldsymbol{r})}{\partial \boldsymbol{r}}\delta\boldsymbol{r} + \frac{\partial \boldsymbol{g}(\boldsymbol{r}, \boldsymbol{n}_o^i)}{\partial \boldsymbol{r}}\delta\boldsymbol{r} + \sum_{i=1}^{4} \frac{\partial \boldsymbol{g}(\boldsymbol{r}, \boldsymbol{n}_o^i)}{\partial \boldsymbol{n}_o^i}\frac{\partial \boldsymbol{n}_o^i}{\partial \boldsymbol{u}}\delta\boldsymbol{u} \tag{21}$$

where

Table 2 Passively stable configurations for different orbits

ρ_0, AU	z_0, AU	β_0	γ_1, rad	θ_1, rad	α_1, rad
0.98	0.001	0.0575055	2.0538	2.0551	0.5175
0.98	0.01	0.0598657	1.42837	2.20700	0.305501
0.96	0.01	0.1150923	2.57570	2.54044	0.194595
0.96	0.02	0.1183463	2.42703	3.00408	0.173011
0.96	0.03	0.1238673	2.80475	2.72312	−0.078137

$$\partial \boldsymbol{f}(\boldsymbol{r})/\partial \boldsymbol{r} = -(\mu/r^3)\boldsymbol{I}_{3\times3} + 3(\mu/r^5)\boldsymbol{r}\boldsymbol{r}^T \tag{22}$$

$$\frac{\partial \boldsymbol{g}(\boldsymbol{r}, \boldsymbol{n}_i)}{\partial \boldsymbol{r}} = 2\sigma S\beta\frac{\mu}{r^4}\left[(\boldsymbol{n}_1\cdot\boldsymbol{r})\boldsymbol{n}_1\boldsymbol{n}_1^T - 2\frac{(\boldsymbol{n}_1\cdot\boldsymbol{r})^6\boldsymbol{n}_1\boldsymbol{r}^T}{r^2} + (\boldsymbol{n}_2\cdot\boldsymbol{r})\boldsymbol{n}_2\boldsymbol{n}_2^T - 2\frac{(\boldsymbol{n}_2\cdot\boldsymbol{r})^6\boldsymbol{n}_2\boldsymbol{r}^T}{r^2} + (\boldsymbol{n}_3\cdot\boldsymbol{r})\boldsymbol{n}_3\boldsymbol{n}_3^T - 2\frac{(\boldsymbol{n}_3\cdot\boldsymbol{r})^6\boldsymbol{n}_3\boldsymbol{r}^T}{r^2} + (\boldsymbol{n}_4\cdot\boldsymbol{r})\boldsymbol{n}_4\boldsymbol{n}_4^T - 2\frac{(\boldsymbol{n}_4\cdot\boldsymbol{r})^6\boldsymbol{n}_4\boldsymbol{r}^T}{r^2}\right]/[4\sigma S + m_1 + m_2] \tag{23}$$

$$\frac{\partial \boldsymbol{g}(\boldsymbol{r}, \boldsymbol{n}_i)}{\partial \boldsymbol{n}_i} = \sigma S\beta\frac{\mu}{r^4}[(\boldsymbol{n}_i\cdot\boldsymbol{r})^2\boldsymbol{I}_{3\times3} + 2(\boldsymbol{n}_i\cdot\boldsymbol{r})\boldsymbol{n}_i\boldsymbol{r}^T] /[4\sigma S + m_1 + m_2] \tag{24}$$

The Jacobian matrices associated with the linearized equations are identified by evaluating these partials along the reference equilibrium state. Then, the variational equations can be written in standard state-space form as

$$\dot{\boldsymbol{X}} = A\boldsymbol{X} + B\delta\boldsymbol{u} \tag{25}$$

where $\boldsymbol{X} = [\,\boldsymbol{r}^T \quad \dot{\boldsymbol{r}}^T\,]^T$, and A and B are constant matrices associated with the initial equilibrium state (i.e., displaced orbit).

Equation (25) is representative of a linear time invariant system. If the distance between two points that represent two different displaced orbits is small, the linear model can be used to solve the transfer problem. To identify an optimal control law, based on the linearized dynamics, the following cost index is defined:

$$J = \frac{1}{2}\int_0^{t_f} (\boldsymbol{X}^T Q\boldsymbol{X} + \delta\boldsymbol{u}R\delta\boldsymbol{u})\,\mathrm{d}t \tag{26}$$

where the weighting matrices Q and R are selected as symmetric positive definite. The time span t_f is specified by the designer. To simplify the solution process, let $\boldsymbol{Y} = [\,\boldsymbol{X}^T \quad \boldsymbol{\lambda}^T\,]^T$ denote an augmented state. Then, the differential equation that describes the evolution of the augmented linear system is given by

$$\dot{\boldsymbol{Y}} = K\boldsymbol{Y} = \begin{bmatrix} A & -BR^{-1}B^T \\ -Q & -A^T \end{bmatrix}\boldsymbol{Y} \tag{27}$$

The solution of Eq. (27) is well known [26] and can be expressed in terms of transition matrix $\Phi(t, 0)$, given by

$$\boldsymbol{Y}(t) = \Phi(t, 0)\boldsymbol{Y}(0) \tag{28}$$

Because K is a constant matrix and diagonalizable here, the transition matrix is therefore analytically determined as

$$\Phi(t,0) = e^{Kt} = e^{P\Lambda P^{-1}t} = Pe^{\Lambda t}P^{-1} = P\begin{bmatrix} e^{\lambda_1 t} & \cdots & 0 \\ \vdots & \ddots & \vdots \\ 0 & \cdots & e^{\lambda_{12}t} \end{bmatrix}P^{-1} = \begin{bmatrix} \Phi_1(t) & \Phi_2(t) \\ \Phi_3(t) & \Phi_4(t) \end{bmatrix} \tag{29}$$

where $\lambda_i = (i = 1 \cdots 12)$ denotes an eigenvalue of matrix K. Λ is a diagonal matrix formed by the eigenvalues of K, and P is formed by the corresponding eigenvectors. Letting $t = t_f$, Eq. (28) can be written as

$$\begin{bmatrix} \boldsymbol{X}_f \\ \boldsymbol{\lambda}_f \end{bmatrix} = \begin{bmatrix} \Phi_1(t_f) & \Phi_2(t_f) \\ \Phi_3(t_f) & \Phi_4(t_f) \end{bmatrix}\begin{bmatrix} \boldsymbol{X}_0 \\ \boldsymbol{\lambda}_0 \end{bmatrix} \tag{30}$$

Because the sailcraft is assumed to start at an equilibrium point, the initial state is defined as $\boldsymbol{X} = 0$. The initial value of the costate

variable is obtained without the need for integration and iterations. Only the eigenvalues and eigenvectors of a 12-dimensional matrix are necessary for this determination. Subsequently, the initial augmented state is determined as

$$\boldsymbol{\lambda}_0 = \Phi_2^{-1}(t_f)[\boldsymbol{X}_f - \Phi_1(t_f)\boldsymbol{X}_0] \tag{31}$$

Therefore, the initial values of the state and costate variables are known and the extended equation can be numerically integrated. The history of the costate variable is stored, and the control action is determined by $\delta\boldsymbol{u} = R^{-1}B^T\boldsymbol{\lambda}$.

The control law in Eq. (31) is specifically targeted to achieve the desired goals in the linearized model. There is no guarantee of success when this control law is implemented in the nonlinear model. Thus, a methodology is necessary to transition the linearized results into the nonlinear model. The objective of the transfer mission is to transition the sailcraft from the initial fixed point (in the rotating frame) $\boldsymbol{X}_0$ to a desired target state $\boldsymbol{X}_T$ through some control action. An iterative differential corrections process is employed to obtain the exact initial costate for the nonlinear model. The iterative process consists of three fundamental steps:

1) The initial costate is obtained from the linear result in Eq. (31).

2) With the control law generated by the initial costate in step 1, the final position, denoted as $\boldsymbol{X}_f$, is calculated by integrating the nonlinear system.

3) The costate is updated with the consideration of Eq. (31):

$$\boldsymbol{\lambda}_0 = \boldsymbol{\lambda}_0 + \Phi_2^{-1}(t_f, 0)(\boldsymbol{X}_T - \boldsymbol{X}_f) \tag{32}$$

The iterative process continues until the error between $\boldsymbol{X}_f$ and $\boldsymbol{X}_T$ is within the specified value.

Numerical simulations: Consider an initial Earth-synchronous displaced orbit characterized by $\rho_0 = 0.98$ AU, $z_0 = 0.001$ AU, and $\omega = \omega_E$. Similarly, let the target orbit be defined by $\rho_0 = 0.982$ AU, $z_0 = 0.002$ AU, and $\omega = \omega_E$. The user-specified transfer time is assumed to be 40 days. The parameters for the passive stability of the sailcraft on the displaced orbit are given in Table 1. The time histories of the four angles are shown in Fig. 6, and the transfer trajectory is shown in Fig. 7. A continuous control law is obtained, and the only small variations of the attitude angles are required to achieve the transfer arc. The angle deviation in the direction perpendicular to plane formed by $\boldsymbol{r}_0$ and z is much smaller than the others, which makes the transfer arc not far from the plane formed by $\boldsymbol{r}_0$ and z.

Several examples with small differences between the two orbits are also tested for the method. The results show that the algorithm works well when the two orbits are close to each other. The differential corrections process achieves the desired accuracy with several iterations. The number of iteration steps increases with the distance between the initial and target states until the process is no longer able to converge with the desired degree of accuracy. In addition, the position and velocity errors at the target point increase with the distance when the distance is outside the linear range. In these cases, the corrections process generates a control law that navigates the sailcraft to a nearby point instead of the target point. Therefore, the linear method cannot achieve the desired transfer arc when the distance is outside the linear range. To circumvent this difficulty, an alternate approach that employs genetic algorithms to identify the optimal control law in the nonlinear system is investigated.

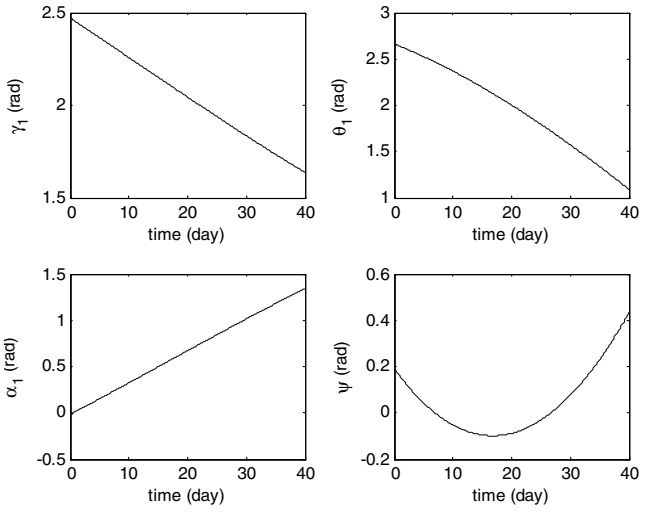

Fig. 6 Control histories for the transfer.

Direct Method for Transfer Trajectory Design

When the distance between two orbits is large, the aforementioned methodology is unsuccessful. An alternate approach is implemented in the nonlinear system to identify the near-time-optimal transfer arc. The literature on low-thrust time-optimal control is extensive. Primarily, there are two methods for solving the resulting nonlinear optimal control problem: indirect and direct. In an indirect method, first-order necessary conditions for optimality are derived from the optimal control problem via the calculus of variations. The primary advantages of indirect methods are their high accuracy and the assurance that the solution satisfies the first-order optimality conditions. However, indirect methods also suffer from several disadvantages, including small radii of convergence and the need for an accurate initial guess for the costate. A direct method has a better convergence compared with an indirect method. In a direct method, the problem is parameterized by discretizing the trajectory and control variables; implicit [27,28] or explicit [29,30] numerical integration schemes are used to satisfy the dynamical constraints. In this study, a direct shooting method is adopted to solve the problem. The control variables are parameterized along the transfer trajectory to minimize the transfer time. The trajectory is divided into segments. Over each segment, the control variables are treated as constant and the differential equations are integrated forward numerically. The control variables and the total fight time are optimized to ensure that the sailcraft arrives at the target point while minimizing the flight time. To avoid local optimal results, a genetic algorithm is employed to obtain the solution for a fixed number of segments. For N-segment division, the problem has $4N + 1$ parameters for the transfer, which can be written as

$$\boldsymbol{Y} = [\,\gamma_1^1 \quad \theta_1^1 \quad \alpha_1^1 \quad \psi^1 \quad \cdots \quad \gamma_1^N \quad \theta_1^N \quad \alpha_1^N \quad \psi^N \quad t_f\,]^T \tag{33}$$

Aside from minimizing the transfer time, the implementation of a genetic algorithm for trajectory optimization requires that the accuracy of the trajectory with respect to the terminal constraints be treated as a secondary optimization objective. This is to ensure that the terminal constraints are satisfied through the search process. In this case, the fitness function must include the transfer time as well as the final distance to the target orbit and the final velocity relative to the target orbit,

$$J = t_f + \kappa_1|\boldsymbol{r}_0 - \boldsymbol{r}_f| + \kappa_2|\dot{\boldsymbol{r}}_0 - \dot{\boldsymbol{r}}_f| \tag{34}$$

where κ_1 and κ_2 are penalty factors for the final time constraints.

To prevent one sail from entering the shadow of another, the angles between the opposite sails should be larger than some critical value and smaller than π. Thus, the optimization parameters should satisfy the following constraints

$$\begin{cases} \gamma_{\min} \le \gamma_1^i \le \pi \\ \gamma_{\min} \le \theta_1^i \le \pi \end{cases} \qquad (1 \le i \le N) \tag{35}$$

The trajectory is integrated using the explicit fourth-order Runge–Kutta method from the initial time to the final time. The fitness function needed to be minimized is calculated at the final time. The parameter optimization problem is stated as follows.

Find optimal $\boldsymbol{Y}$ that minimizes fitness function J subject to state equation $\ddot{\boldsymbol{r}} + 2\boldsymbol{\omega}_0 \times \dot{\boldsymbol{r}} + \boldsymbol{\omega}_0 \times (\boldsymbol{\omega}_0 \times \boldsymbol{r}) = \boldsymbol{f}(\boldsymbol{r}) + \boldsymbol{g}(\boldsymbol{r}, \boldsymbol{n}_o^i)$ and inequality constraints

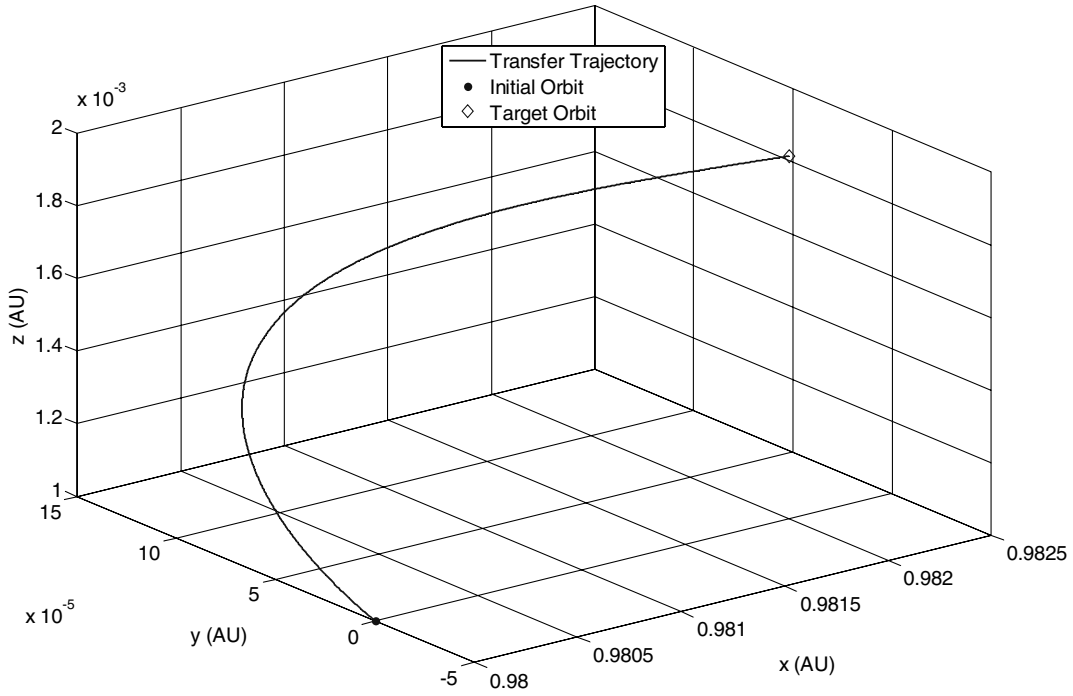

Fig. 7 Transfer trajectory for the linear control.

$$\begin{cases} \gamma_{\min} \le \gamma_1^i \le \pi \\ \gamma_{\min} \le \theta_1^i \le \pi \end{cases} \qquad (1 \le i \le N)$$

where the initial condition $\boldsymbol{X}(0) = \boldsymbol{X}_0$ is given.

The genetic algorithm software package in MATLAB® 7.1 is used to solve the optimization problem. The necessary fitness function, optimization variables, and parameters for the genetic algorithm [31] are given in Table 3. The results indicate that the final time constraints are difficult to satisfy with the genetic algorithm. Therefore, a conjugate gradient method is employed to reduce the position and velocity errors. The optimized parameters obtained by the genetic algorithm are taken as an initial guess to the conjugate gradient method.

Numerical simulations: The initial and target Earth-synchronous orbits are defined by $\rho_0 = 0.98$ AU, $z_0 = 0.001$ AU and $\rho_0 = 0.96$ AU, $z_0 = 0.02$ AU, respectively. The parameters for the sailcraft are given in Table 1. The transfer trajectory is divided into five segments and 21 optimization parameters are optimized. The parameters of the genetic algorithm are adjusted for different optimization runs. Several groups of parameters generate very close solutions that are more optimal than others. One group of the parameters is given in Table 3, and the results of the process are shown in Table 4. When the sailcraft arrives at the target orbit, it adjusts its configuration to achieve passive stability. However, the results in [18] show that position and velocity errors lead to the deviation of a sailcraft's orbit from the target orbit. The maximum distance between the sailcraft and the target orbit increase with position and velocity errors. The sailcraft remains in the vicinity of the orbit when the errors are small, and large errors lead to instability. The results in Table 4 show that the final position error is about

Table 3 Parameters for the genetic algorithm

Genetic algorithm	Parameter value
Population size	40
Creation function	Uniform
Selection function	Stochastic uniform
Mutation function	Uniform (0.4487)
Crossover function	Heuristic (1.2)
Generation	700

Table 4 Results of the genetic algorithm

	γ_1^i, rad	θ_1^i, rad	α_1^i, rad	ψ^i, rad	t_f, day	$\lvert\boldsymbol{r}_o - \boldsymbol{r}_f\rvert$, km	$\lvert\dot{\boldsymbol{r}}_o - \dot{\boldsymbol{r}}_f\rvert$, km/s
$i = 1$	1.657	2.101	−0.1068	0.5470	——	——	——
$i = 2$	1.896	1.791	−0.08267	−0.3546	——	——	——
$i = 3$	2.483	2.086	0.3232	0.1337	118.93	1078.8	0.8225
$i = 4$	1.940	2.843	0.01798	−0.3643	——	——	——
$i = 5$	2.396	1.719	−0.2293	0.3302	——	——	——

Table 5 Results of the conjugate gradient method

	γ_1^i, rad	θ_1^i, rad	α_1^i, rad	ψ^i, rad	t_f, day	$\lvert\boldsymbol{r}_o - \boldsymbol{r}_f\rvert$, km	$\lvert\dot{\boldsymbol{r}}_o - \dot{\boldsymbol{r}}_f\rvert$, km/s
$i = 1$	1.704	2.056	−0.1392	0.6381	——	——	——
$i = 2$	1.971	1.978	−0.1885	−0.3361	——	——	——
$i = 3$	2.358	2.136	0.2630	0.2258	119.27	3.25e–8	3.83e–14
$i = 4$	2.197	3.136	0.1896	−0.3147	——	——	——
$i = 5$	2.945	2.497	0.2548	0.1034	——	——	——

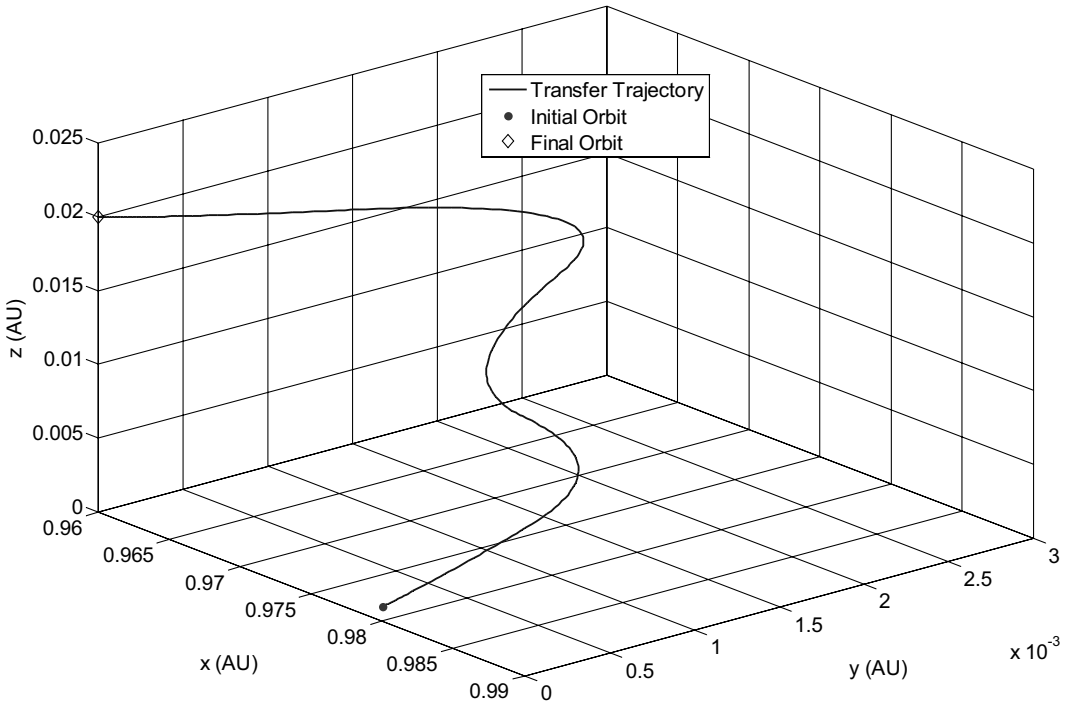

Fig. 8 Transfer trajectory for the direct method.

1000 km and the velocity error is about 1 km/s, which may exceed stability requirements. Therefore, the conjugate gradient method is employed to refine the results and reduce the final errors. The initial values of the optimization parameters are obtained from the optimized parameters of the genetic algorithm. The corresponding results are given in Table 5. The results show that both the position and velocity errors are reduced to be very small. The transfer arc is given in Fig. 8.

In principle, this control law seems disadvantageous because the control law obtained is not continuous. However, such a steering law is likely to be significantly easier to implement for a sailcraft. The sailcraft can evolve along each segment with a fixed attitude, rather than track a continuously changing attitude as required by the linear method. With the control implementation considered, the transfer arc should be divided into as few segments as possible. However, the transfer time increases as the number of the segments decreases. Therefore, a compromise between the transfer time and the segment number should be considered to design the trajectory. The results show that the transfer time is always near the minimum time as long as the number of segments is larger than five.

The advantage of the linear method is that the control law is simple and greatly decreases the computational burden. In our case, the control law is in an analytical form and onboard trajectory optimization is possible. Because it is difficult to derive an analytical control law for a nonlinear model, the LQR method is a bridge to obtain a simple and analytical transfer control law for the nonlinear model though it does not generate a true minimum-time transfer trajectory. The disadvantage is that the linear method is subject to limitation on the distance between the initial and target orbits. In addition, transfer errors exist when this control law is implemented in the nonlinear model. To cancel the transfer errors, a differential correction process is used to transition the results from linear control law into a nonlinear model. When the iterative process does not converge, the distance is beyond the ability of the linear control method. It is hard to determine the exact distance that makes the linear method invalid.

Conclusions

This paper proposed a new sailcraft configuration that has the ability to vary its lightness number. This kind of configuration can be designed as passively stable on different orbits with different locked states. The focus of this investigation is the development of a systematic approach to identify transfer arcs between displaced solar orbits by adjusting the sail orientation for various sailcraft configurations. When the distance between the initial and target orbit is small, a linearized optimal control law is suitable to identify transfers between displaced orbits. However, when the distance between orbits grows larger, the earlier method is ineffective. In this case, a hybrid control strategy is implemented that incorporates a genetic algorithm with a conjugate gradient method to identify the time-optimal transfer between displaced orbits.

Acknowledgments

This work was supported by the National Natural Science Foundation of China (grants 10832004 and 10672084). The authors would like to acknowledge the reviewers' work for the paper.

References

[1] McInnes, C. R., MacDonald, M., Angelopolous, V., and Alexander, David, "GEOSAIL: Exploring the Geomagnetic Tail Using a Small Solar Sail," *Journal of Spacecraft and Rockets*, Vol. 38, No. 4, 2001, pp. 622–629. doi:10.2514/2.3727

[2] West, J. L., and Derbes, B., "Solar Sail Vehicle System Design for the Geostorm Warning Mission," AIAA Paper 2000-5326, 2000.

[3] Prado, J. Y., Perret, A., Pignolet, G., and Dandouras, I., "Using a Solar Sail for a Plasma Storm Early Warning System," International Academy of Astronautics, Paper IAA-96-IAA.3.3.06, Oct. 1996.

[4] Forward, R. L., "Technical Note, Light-Levitated Geostationary Cylindrical Orbits," *Journal of the Astronautical Sciences*, Vol. 29, No. 1, 1981, pp. 73–80.

[5] McInnes, C. R., and Simmons, F. L., "Solar Sail Halo Orbits I: Heliocentric Case," *Journal of Spacecraft and Rockets*, Vol. 29, No. 4, 1992, pp. 466–471. doi:10.2514/3.25487

[6] McInnes, C. R., "Passive Control of Displaced Solar Sail Orbits," *Journal of Guidance, Control, and Dynamics*, Vol. 21, No. 6, 1998, pp. 975–982. doi:10.2514/2.4334

[7] McInnes, C. R., "Solar Sail Mission Applications for Non-Keplerian Orbits," *Acta Astronautica*, Vol. 45, No. 4–9, 1999, pp. 567–575. doi:10.1016/S0094-5765(99)00177-0

[8] Friedman, L., "The Cosmos-1 Solar Sail," *Royal Astronomical Society Discussion Meeting Solar Sail Mission Applications*, Royal

Astronomical Society, London, May, 2002.
[9] Lichodziejewski, D., Derbès, B., Slade, K, and Mann, T., "Vacuum Deployment and Testing of a 4-Quadrant Scalable Inflatable Rigidizable Solar Sail System," AIAA Paper 2005-3927, April 2005.
[10] David, L., Billy, D., and Rich, R., "Development and Ground Testing of a Compactly Stowed Scalable Inflatably Deployed Soar Sail," AIAA Paper 2004-1507, April, 2004.
[11] Gaspar, J. L., Mann, T., Behun, V., Wilkie, K., and Pappa, R., "Development of Modal Test Techniques for Validation of a Solar Sail Design," AIAA Paper 2004-1665, April, 2004.
[12] Wie, B., "Solar Sail Attitude Control and Dynamics, Part 1," *Journal of Guidance, Control, and Dynamics*, Vol. 27, No. 4, 2004, pp. 526–535. doi:10.2514/1.11134
[13] Wie, B., "Solar Sail Attitude Control and Dynamics, Part 2," *Journal of Guidance, Control, and Dynamics*, Vol. 27, No. 4, 2004, pp. 536–544. doi:10.2514/1.11133
[14] Wie, B., and David, M., "Robust Attitude Control Systems Design for Solar Sail, Part 1: Propellantless Primary ACS," *AIAA Guidance, Navigation, and Control Conference and Exhibit*, Vol. 1, AIAA, Reston, VA, 2004, pp. 1–28.
[15] Jordan, E., Michael, L., Peter, W., James, E., Jeff, B., Dan, S., Leonel, R., and Dale, L., "A Solar Sail Integrated Simulation Toolkit," American Astronautical Society Paper 04-283, Feb. 2004.
[16] Gyula, G., "Solar Sail Scalability and the Concept of a 'Truly Scalable' Architecture," AIAA Paper 2006-1703, May 2006.
[17] Gyula, G., and Edward, E. M., "Space Tow Solar Sails—Design Study Exploring Performance and Operational Issues," AIAA Paper 2007-1826, April 2007.
[18] Gong, S. P., Li, J. F., and Baoyin, H. X., "Passive Stability Design for the Solar Sail on Displaced Orbits," *Journal of Spacecraft and Rockets*, Vol. 44, No. 5, 2007, pp. 1071–1079. doi:10.2514/1.29752
[19] McInnes, C. R., "Solar Sail Parking in Restricted Three-Body Systems," *Journal of Guidance, Control, and Dynamics*, Vol. 17, No. 2, 1994, pp. 399–406. doi:10.2514/3.21211
[20] Friedman, L., Pichkhadze, K., Kudryashov, V., Rogovsky, G., Linkin, V., Gotlib, V., Lipatov, A., Cantrell, J., and Garvey, J., "COSMOS 1: the Attempt to Fly the First Solar Sail Mission," IAA Paper 11-1-03, 2002.
[21] McInnes, C. R., "Passive Control of Displaced Solar Sail Orbits," *Journal of Guidance, Control, and Dynamics*, Vol. 21, No. 6, 1998, pp. 975–982. doi:10.2514/2.4334
[22] McInnes, C. R., "Dynamics, Stability, and Control of Displaced Non-Keplerian Orbits," *Journal of Guidance, Control, and Dynamics*, Vol. 21, No. 5, 1998, pp. 799–805. doi:10.2514/2.4309
[23] Baoyin, H. X., and McInnes, C. R., "Solar Sail Orbits at Artificial Sun–Earth Libration Points," *Journal of Guidance, Control, and Dynamics*, Vol. 28, No. 6, 2005, pp. 1328–1330. doi:10.2514/1.14598
[24] Baoyin, H. X., and McInnes, C. R., "Solar Sail Equilibria in the Elliptical Restricted Three-Body Problem," *Journal of Guidance, Control, and Dynamics*, Vol. 29, No. 3, 2006, pp. 538–543. doi:10.2514/1.15596
[25] Biggs, J. D., McInnes, C. R., and Waters, T., "Control of Solar Sail Periodic Orbits in the Elliptic Three-Body Problem," *Journal of Guidance, Control, and Dynamics*, Vol. 32, No. 1, 2009, pp. 318–320. doi:10.2514/1.38362
[26] Bryson, A. E., "Time-Varying Linear-Quadratic Control," *Journal of Optimization Theory and Applications*, Vol. 100, No. 3, 1999, pp. 515–525. doi:10.1023/A:1022682305644
[27] Hargraves, C. R., and Paris, S. W., "Direct Trajectory Optimization Using Nonlinear Programming and Collocation," *Journal of Guidance, Control, and Dynamics*, Vol. 10, No. 4, 1987, pp. 338–342. doi:10.2514/3.20223
[28] Enright, P. J., and Conway, B. A., "Discrete Approximations to Optimal Trajectories Using Direct Transcription and Nonlinear Programming," *Journal of Guidance, Control, and Dynamics*, Vol. 15, No. 4, 1992, pp. 994–1002. doi:10.2514/3.20934
[29] Otten, M., and McInnes, C. R., "Near Minimum-Time Trajectories for Solar Sails," *Journal of Guidance, Control, and Dynamics*, Vol. 24, No. 3, 2001, pp. 632–634. doi:10.2514/2.4758
[30] Hughes, G. W., and McInnes, C. R., "Solar Sail Hybrid Trajectory Optimization for Non-Keplerian Orbit Transfers," *Journal of Guidance, Control, and Dynamics*, Vol. 25, No. 3, 2002, pp. 602–604. doi:10.2514/2.4924
[31] Goldberg, D. E., *Genetic Algorithms in Search, Optimization and Machine Learning*, Addison–Wesley, Redwood City, CA, 1989.

B. Marchand
Associate Editor